coatings

MDPI

Article

The Design and Characterization of New Chitosan, Bioglass and ZnO-Based Coatings on Ti-Zr-Ta-Ag

Mariana Prodana [1], Daniela Ionita [1,*], Andrei Bogdan Stoian [1], Ioana Demetrescu [1,2], Geanina Valentina Mihai [3] and Marius Enăchescu [2,3]

[1] Department of General Chemistry, Univeristy Politehnica of Bucharest, 011061 Bucharest, Romania
[2] Academy of Romanian Scientists, 050094 Bucharest, Romania
[3] Center for Surface Science and Nanotechnology, Univeristy Politehnica of Bucharest, 060042 Bucharest, Romania
* Correspondence: daniela.ionita@upb.ro

Abstract: The starting point of this study is a new alloy with rare metals such as Ta and Zr that has Ag in the composition, proven antibacterial properties. New coatings on Ti-Zr-Ta-Ag capable of improving the alloys' properties and to be suitable for more applications have yet to be fabricated. New formulations based on chitosan (Ch) and bioglass (BG) were designed as multifunctional coatings to be deposited from suspensions on the mentioned alloy. To make the suspensions used for deposition, several samples were made containing Ch, BG and ZnO in various mass ratios. A number of solutions with different component ratios were produced and analyzed by ζ potential and Dynamic Light Scattering (DLS) to determine the most stable mixture, which was subsequently deposited on the Ti-Zr-Ta-Ag samples. The mixtures and the samples obtained after applying the coating were characterized from a morphological and compositional standpoint using Scanning Electron Microscopy coupled with energy dispersive X-ray spectroscopy (SEM-EDX) and Fourier-transform infrared spectroscopy (FT-IR). Further analyses on the properties of the coating were performed using contact angle and roughness analysis. Zeta potential measurements demonstrated evidence of a good stability of the coatings. The size of the ceramic particles is between 1 and 10 µm. From the SEM, the morphology of all the components from the mixture containing chitosan, bioglass and ZnO are shown to be present on the surface. From the FTIR determination, all the functional groups that appear demonstrated evidence of the presence of BG, ZnO and chitosan. The contact angle values of the coated samples are in the hydrophilic domain but are higher compared to the uncoated alloy values. Such behavior is promising in a potential bioapplication.

Keywords: bioglass; chitosan; zinc oxide; multifunctional coatings; titanium alloy

Citation: Prodana, M.; Ionita, D.; Stoian, A.B.; Demetrescu, I.; Mihai, G.V.; Enăchescu, M. The Design and Characterization of New Chitosan, Bioglass and ZnO-Based Coatings on Ti-Zr-Ta-Ag. *Coatings* **2023**, *13*, 493. https://doi.org/10.3390/coatings13030493

Academic Editor: Fengwei (David) Xie

Received: 30 January 2023
Revised: 14 February 2023
Accepted: 21 February 2023
Published: 23 February 2023

1. Introduction

Starting in the middle of the last century, titanium was the most selected metallic material for many applications [1–4] in various environments, including bioliquids [5–7] due to its remarkable properties regarding its electrochemical stability and mechanical characteristics. Most of the metallic alloys used for implantology are based on titanium and stainless steel and used mainly in the orthopedic field due to their good mechanical properties. The need to enhance the mechanical properties of pure titanium for various fields of applications has led to the elaboration and use of alloys such as TiAlV and TiAlNb which have been homologated [8,9] and used intensively as biomaterials [10]. The toxicity generated by ions that could be released from the metallic surface into the human body fibrous structures [5,6] of Al and V, which are present in such approved alloys, has led, at the beginning of this century, to the promotion of binary titanium alloys with Zr [11,12], one of the most biocompatible elements of the system. In looking for more performant metallic materials, a new class of multicomponent alloys (or high entropy

alloys) was developed [13,14]. These alloys are formed with at least five principal elements in equiatomic or near-equiatomic proportions that lead to a single-phase solid solution. In the last years, high entropy alloys (HEAs) and medium entropy alloys (MEAs) were elaborated based on Fe, Zr, Ti and rare metals [15], keeping in their content elements with a very good biocompatibility. The alloy used in this work is one such example with Ti, Ta and Zr [16] containing a small amount of Ag, intended to enhance the antibacterial properties. The microstructure and characteristics of the new alloy have been established and, for better performance, its surface was modified at micro- and nano-level depending on the proposed application [17–19].

To prevent toxicity, coatings of the metallic surfaces are widely applied, having the ability to increase osteointegration and decrease ion release concentration. To obtain new materials with good biocompatibility using the coating method, bioactive materials are needed. Coatings such as hydroxyapatite (HA) [20–22], bioactive glass (BG) and glass-ceramic [23–28] composite materials based on biopolymers and ceramic materials [29,30] are commonly used. HA-based materials act like a bone composed of collagen as an organic phase and an inorganic phase [31]. Hybrid materials also use biopolymers, such as alginate or chitosan (Ch), and ceramic particles as a bioactive glass with good mechanical properties and biocompatibility [32]. Active molecules, antibiotics, proteins and enzymes can also be attached to the hybrid sustainable coatings [32,33]. For biomedical applications, bioactive glass is an important type of coating, having the possibility to form chemical bonds with the surrounding tissue. Bioactive glass was discovered by Hench and coworkers in the late 1960s and early 1970s and is known as 45S5 or Bioglass® [34,35]. To increase the biocompatibility of the glass, boron is incorporated [36]. In bioactive glass coatings, chitosan is used as an organic phase, derived from chitin, a natural polymer with antibacterial properties [37]. The electrophoretic deposition (EPD) in the aqueous electrolyte is one of the methods used in this regard [38] to produce hybrid coatings for dental and orthopedical application [39–42].

The purpose of this paper is to obtain new multifunctional coatings based on chitosan, bioglass and ZnO. In this study, the deposition is carried out on a 73Ti-20Zr-5Ta-2Ag alloy. Using coatings with carefully selected materials as a strategy for improving the surface material properties was one of the aims of this study. Such experiments represent novel investigations entirely and new formulations based on chitosan (Ch), bioglass (BG) and ZnO were proposed as multifunctional coatings to be deposited. The suspensions used for deposition were studied in detail, determining the stability of the particles in suspension.

The surface analysis coupled with compositional and structural techniques completed this paper's investigations.

The research hypothesis and the investigation motivation in selecting this alloy to be coated is based on previous knowledge that, being an MEA, this alloy has better mechanical properties, much closer to human bone than conventional alloys. Studies of coatings on this particular alloy were never presented in previous papers and the formulation with well-selected biocompatible components elaborated and characterized in this study could lead to the improvement in implant applications.

2. Materials and Methods

2.1. Substrate Preparation

73Ti-20Zr-5Ta-2Ag alloy samples (Ø20 mm × 1 mm) were polished using SiC paper with increasing grits from P800 to P3600 (Buehler, Lake Bluff, IL, USA), cleaned in an ultrasonic bath with acetone, ethanol and distilled water 10 min each, then etched by immersion in an acid mixture of 3HNO3:1HF:2H2O (volume ratios) for 10 s. A control sample (henceforth P0) was preserved for surface analysis.

2.2. Solution Preparation and Film Deposition

Chitosan (190–310 kDa, 78–85% deacetylation, Sigma-Aldrich, Saint Louis, MO, USA), pure water (Purelab Option R7BP, ELGA, High Wycombe, UK), acetic acid (Sigma-Aldrich),

bioglass (BG-45S5, 0.2-250 µm) and ZnO (<50 nm) were used to prepare the suspension. The chitosan (0.5 g/L w/v) was dissolved in 1% acetic acid solution under stirring for 4 h. BG and ZnO were added to the chitosan solution in various mass ratios. In Table 1, the mixtures fabricated for this work are listed. In order to obtain an adequate dispersion of the suspension components, the mixture was magnetically stirred for 60 min, then ultrasonicated for 60 min.

Table 1. List of fabricated samples and components.

Sample	Components	Chi:(BG:ZnO) Ratio (w/w)	BG:ZnO Ratio (w/w)
P1	Ti-Zr-Ta-Ag/Chi	-	-
P2	Ti-Zr-Ta-Ag/Chi/(BG/ZnO)	1:1	5:1
P3	Ti-Zr-Ta-Ag/Chi/(BG/ZnO)	1:1	1:1
P4	Ti-Zr-Ta-Ag/Chi/(BG/ZnO)	1:1	1:5
P5	Ti-Zr-Ta-Ag/Chi/(BG/ZnO)	2:1	1:5
P6	Ti-Zr-Ta-Ag/Chi/(BG/ZnO)	2:1	1:1
P7	Ti-Zr-Ta-Ag/Chi/(BG/ZnO)	2:1	5:1

The mixture with the best results after zeta potential (ζ-potential) and dynamic light scattering (DLS) testing was then coated by using a high-power source (PS/EJ30P20, Glassman High Voltage, Inc., High Bridge, NJ, USA) connected to a pump (Legato 180, KD Scientific, Holliston, MA, USA) on 73Ti-20Zr-5Ta-2Ag-etched surfaces and then tested further. The parameters for the deposition were applied voltage 20 kV, flow rate 0.5 mL/h, needle to sample distance 10 cm.

The sample preparation process is schematically represented in Figure 1.

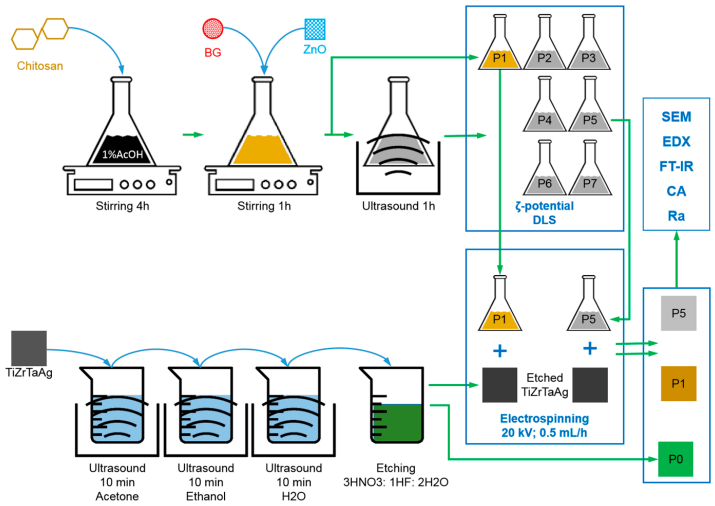

Figure 1. Schematic representation of sample preparation process.

2.3. Sample Characterization

The ζ-potential was measured for the suspension used to coat the alloy samples by microelectrophoresis (Zetasizer Nano ZS, Malvern Instruments Inc., Malvern, UK). Before analysis, the suspensions were diluted 1:100 (v/v) with deionized water. The electric charge (ζ-potential) was determined by imputing the measured electrophoretic mobility of the suspended particles in the Helmholtz–Smoluchowski Equation (1).

$$\zeta = EM\frac{4\pi\eta}{\varepsilon} \quad (1)$$

where ζ = zeta potential, *EM* = electrophoretic mobility, η = viscosity of the dispersion solution, ε = the dielectric constant.

The ζ-potential can be used to determine the stability of suspended particles and can be controlled by the addition of acids, bases, ion absorption or polyelectrolytes. A low ζ-potential value is a sign of particle agglomeration, and a high ζ-potential value is a sign of a lack of sedimentation [43–47].

The particle size was estimated by DLS using a Zetasizer Nano ZS size analyzer (Malvern Instrument, Ltd., Malvern, UK) with parameters adjusted for each sample. The equivalent spherical diameter of the particles in the suspension is calculated by applying the Stokes–Einstein Equation (2).

$$d = \frac{kT}{3\pi\rho D} \quad (2)$$

where d = spherical diameter, k = Boltzmann constant, T = absolute temperature, ρ = viscosity of the dispersion solution, D = particle diffusion coefficient.

The morphology of the samples was analyzed by Scanning Electron Microscopy (SEM) using a Hitachi SU 8230 (HITACHI High-Technologies Corporation, Tokyo, Japan) equipped with Energy Dispersive X-ray (EDX) analyzer (Oxford Instruments, Abingdon, UK) using an accelerating voltage of 10 kV, a chamber pressure of approx. 8×10^{-4} Pa and a working distance of approx. 9 mm.

Fourier transform infrared spectroscopy (FT-IR) analysis was performed using a Perkin-Elmer Spectrum 100 (Perkin-Elmer, Shelton, CT, USA), in absorbance mode, in the range 600–4000 cm^{-1}.

Roughness determinations were performed using an RT1200 roughness tester (PCE Instruments, Southampton Hampshire, UK).

Contact angle measurements were performed using a CAM100 optical contact angle equipped with a surface tension meter from (KSV Instruments—Espoo, Finland). Static contact angle measurements were performed using ultrapure water. An amount of 5 μL droplets was placed on the surface of the samples and the contact angle values were measured immediately after droplet placement. The values represent the median of 5 measurements.

3. Results

3.1. Zeta Potential and Average Particle Size

In Figure 2, the ζ-potentials of the suspensions used to coat the alloy samples are presented. All the mixtures had a good stability; however, a slight decrease in the stability was observed with the increase in the ceramic component, this behavior being due to the large dimensions of the BG. The addition of ZnO led to an increase in the stability due to the overall positive charge of the ZnO particles [48]. The positive value of the ζ-potential also supports the presence of chitosan on the surface of the prepared nanocomposite since the chitosan is positively charged [49].

Statistical comparisons of the ζ-potential data groups were analyzed by Beanplot [50] (Figure 1). Broadly, the samples can be divided into three groups: Group 1 containing only the control sample P1, Group 2 represented by samples P2, P3 and P4 with the 1:1 Chi:(BG:ZnO) ratio which show similarities and Group 3 represented by the samples P5, P6 and P7 with the 2:1 Chi:(BG:ZnO) ratio. Apart from the control sample P1, the sample which shows the greatest difference from the others is sample P5. The observed increase in the ζ-potential values for P5 can be attributed to the synergistic effect given by the greater quantities of ZnO and chitosan which are positively charged.

The highest stability was detected for sample P5 with a ζ-potential of 74.6 mV, the first signs of sedimentation appearing after approximately 102 h. The DLS results for the mixtures used to coat the alloy samples (Figure 3) show that the mean size of the particles (D_{50} Z-ave) is approximately in the range 0.9–2.5 μm. The smallest Z-ave values were observed for P5. The sedimentation rate of a suspension depends on the size of the particles, the shape, density as well as on the viscosity of the fluid in which they are

suspended. Smaller particle sizes lead to a longer sedimentation time. The high stability of P5 was probably due to the higher polymer to ceramic ratio, which prevented the agglomeration of the suspended particles.

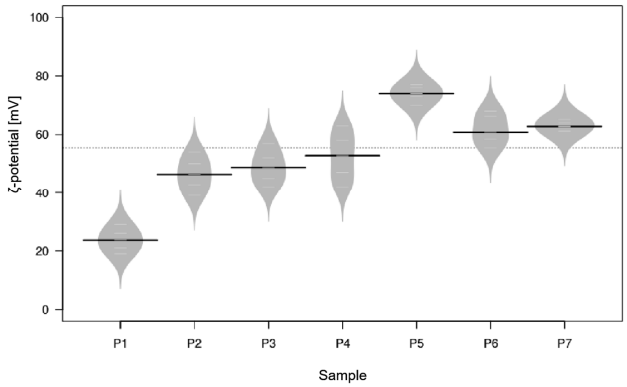

Figure 2. Beanplot graph obtained for the samples.

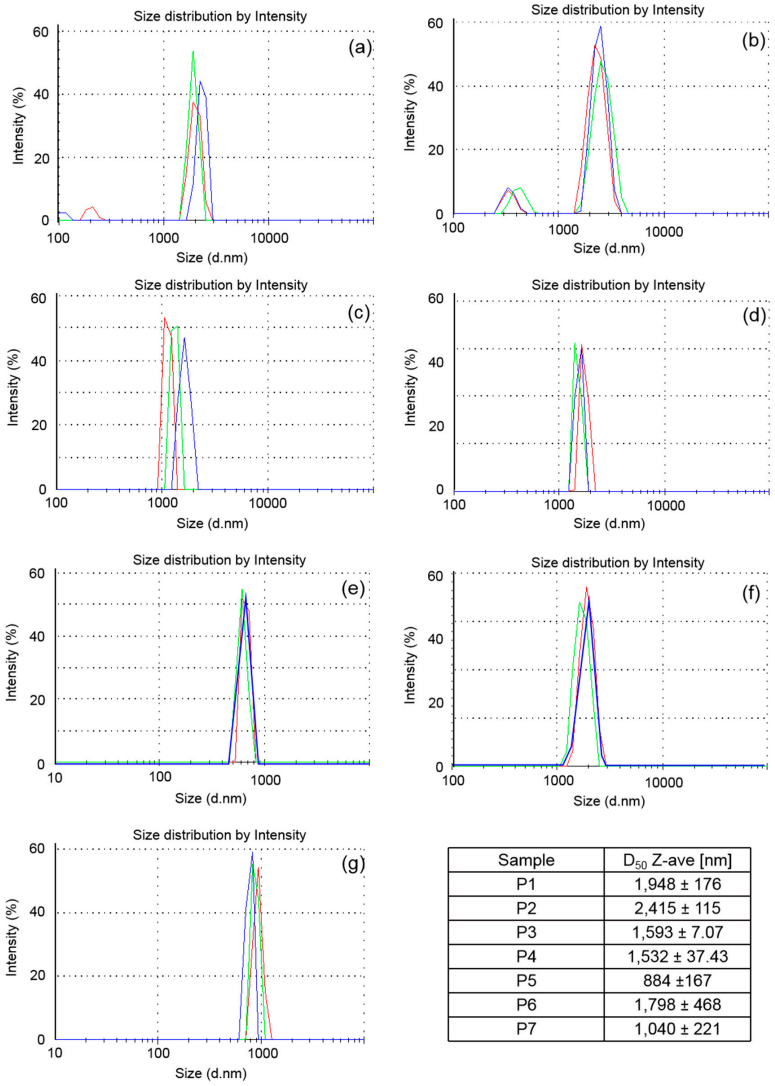

Sample	D_{50} Z-ave [nm]
P1	1,948 ± 176
P2	2,415 ± 115
P3	1,593 ± 7.07
P4	1,532 ± 37.43
P5	884 ±167
P6	1,798 ± 468
P7	1,040 ± 221

Figure 3. DLS spectra obtained for (**a**) P1; (**b**) P2; (**c**) P3; (**d**) P4; (**e**) P5; (**f**) P6; (**g**) P7 and average particle sizes from three measurements for each sample.

3.2. Surface Morphology

For the surface morphology analysis, three samples were selected: P0—the reference sample, P1—the alloy coated with chitosan and P5—the sample with the optimum ζ-potential value and longest sedimentation time.

The control samples' (P0) surface (Figure 4a) is covered with complex oxides resulting from the etching process. Small (0.7–1 µm) silver formations are present, scattered on the surface and visible as bright regions in the images. The formations seem to have a tendency for agglomeration, many of them being present on the surface as clusters. Clustered nanopores of around 400–500 nm were observed in the metallic oxide stratum.

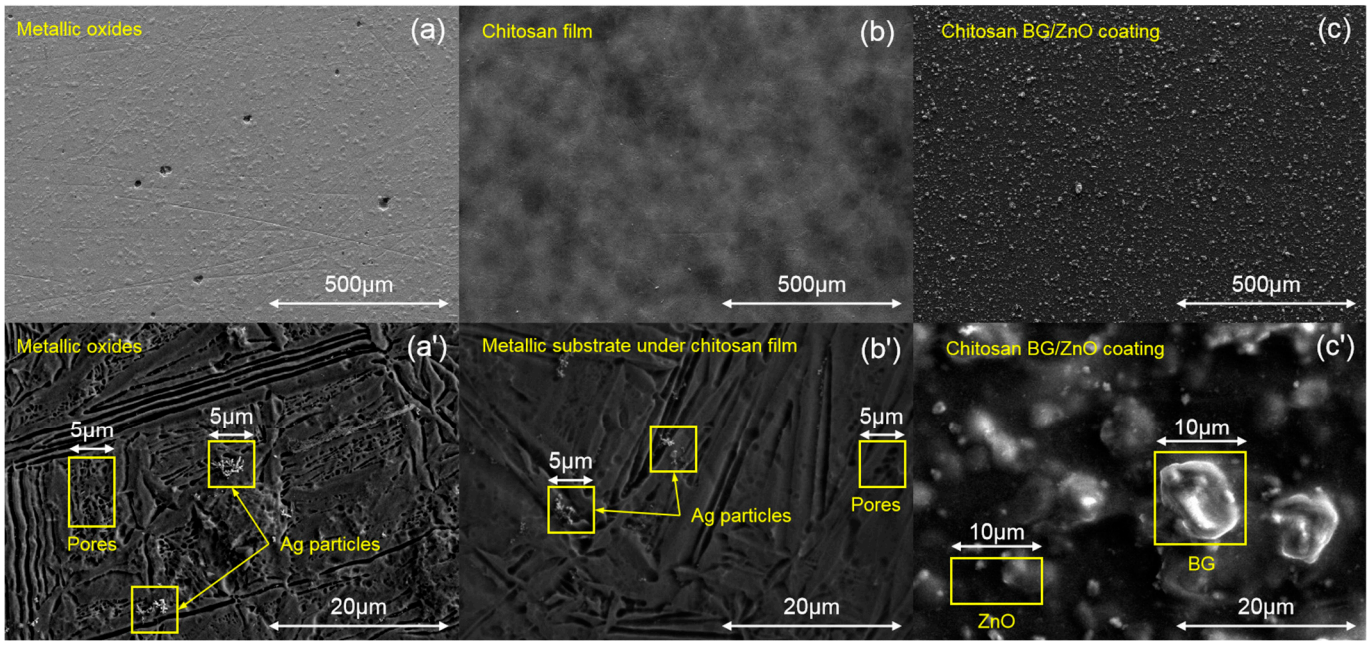

Figure 4. SEM micrographs for (**a**,**a'**) P0; (**b**,**b'**) P1; (**c**,**c'**) P5.

The surface of sample P1 (Figure 4b) is covered with a thin chitosan film. The electron beam could penetrate the film, so the metallic oxide structures from beneath are visible at higher magnifications.

On the surface of sample P5 (Figure 4c), the ceramic particles are well dispersed in the polymeric matrix, with sizes between 1 and 10 µm. It seems that during the deposition or drying process, the agglomeration of particles occurred, leading to larger particle sizes than in the dispersion.

3.3. Coating Composition

Energy dispersive X-ray spectroscopy (EDX) was used to determine the composition of the surfaces of the samples. In Figure 3, the EDX spectra and relative atomic weight composition for three representative samples are presented. The surface of sample P0 (Figure 5a) is mainly composed of metallic oxides produced after the etching process. Sample P1 (Figure 5b) shows the increase in carbon percentage from the coating with the chitosan solution. On sample P5 (Figure 5c), all the components from the mixture containing chitosan, bioglass and ZnO are shown to be present on the surface.

FT-IR analysis (Figure 6) was performed for each suspension component, their mixture and alloy samples both bare and covered. Characteristic IR absorption peaks of functional groups could be identified and attributed for each component.

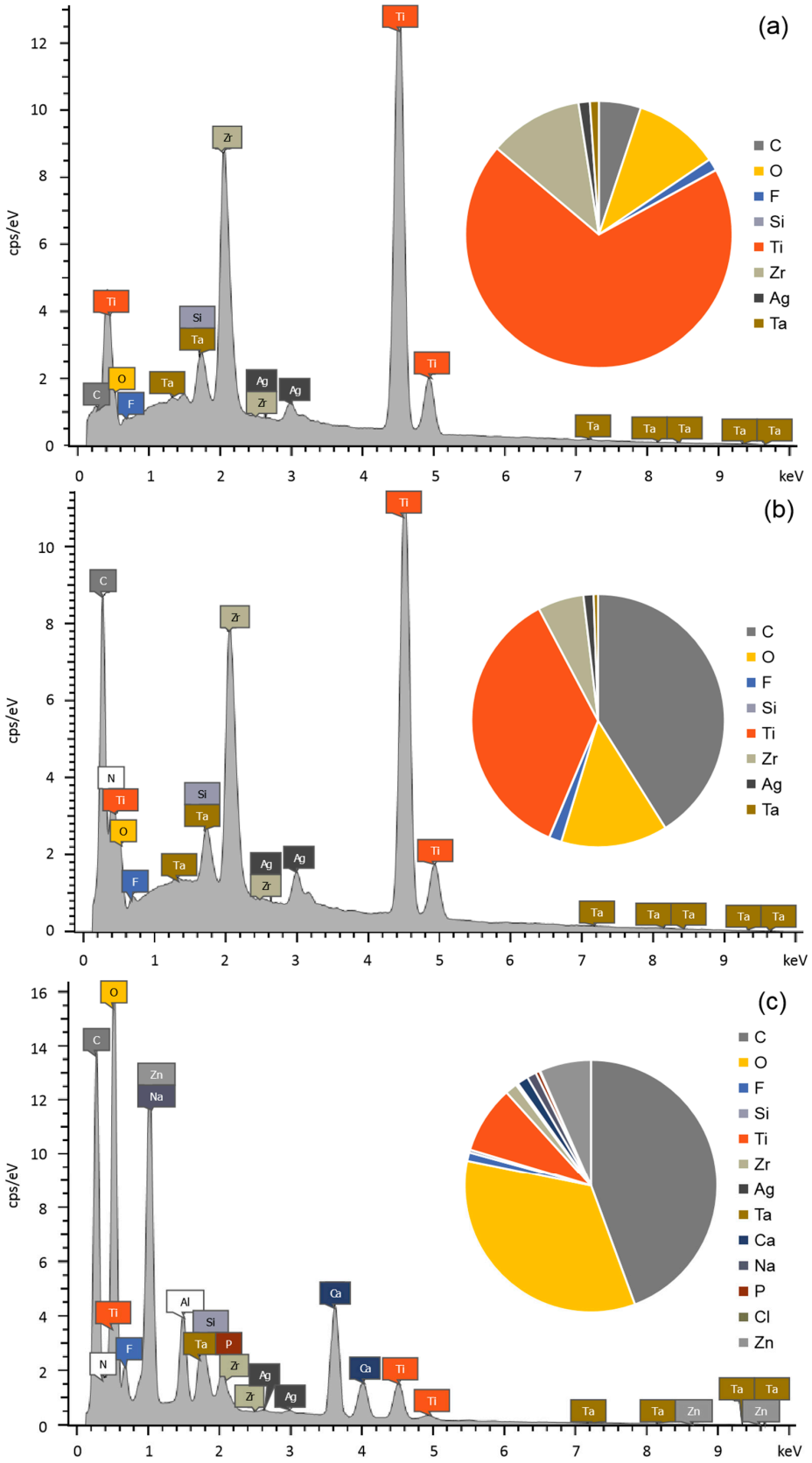

Figure 5. EDX spectra and elemental composition for (**a**) P0; (**b**) P1; (**c**) P5.

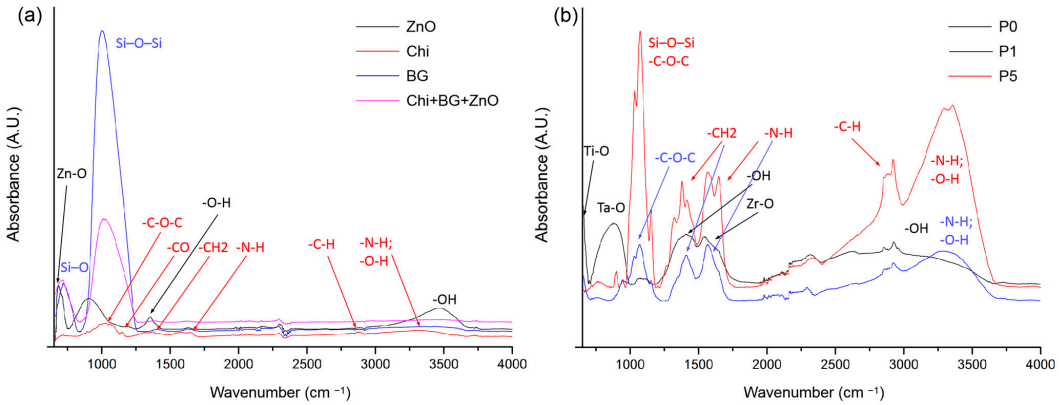

Figure 6. FT-IR spectra obtained for (**a**) mixture components; (**b**) Ti-Zr-Ta-Ag samples.

For the ZnO powder, the peak found at 625 cm^{-1} was attributed to Zn-oxygen stretching and an O-H stretching peak from absorbed water molecules was observed at 3700–3184 cm^{-1}. The following peaks were attributed to chitosan particles: C-O-C stretching at 1001 cm^{-1}, C-O stretching at 1066 cm^{-1}, CH_2 bending at 1423 cm^{-1}, N-H bending at 1645 cm^{-1}, C-H stretching at 2877 cm^{-1} and N-H and O-H stretching at 3291–3361 cm^{-1} [51]. The bioglass powder has characteristic peaks at 800 cm^{-1} and 1001 cm^{-1}, attributed to Si-O vibration and Si-O-Si vibration, respectively. For the etched uncovered Ti-Zr-Ta-Ag alloy, the following peaks were attributed: Ti-O stretching at 690 cm^{-1}, Ta-O stretching at 750 cm^{-1} and Zr-O stretching at 1500 cm^{-1}. The peaks at 1420–1330 cm^{-1} and 3700–3184 cm^{-1} were attributed to O-H bending and O-H stretching from water molecules [52,53]. When the covered Ti-Zr-Ta-Ag alloy samples were analyzed, all the peaks from the different mixture components were present.

3.4. Contact Angle and Surface Roughness

The contact angle and surface roughness of all the samples are presented in Figure 7. The increase in the contact angle in the case of the chitosan coating can be attributed to the molecular structure of chitosan. Probably, the absence of groups capable of hydrogen bonds on the surface of the chitosan film can explain the often-observed hydrophobic nature of the chitosan films. The addition of the ceramic mixture leads to an increase in the contact angle, as can be seen from the experimental determinations. The surface roughness can be correlated with the SEM morphology, noting that the coatings containing larger particles lead to obtaining surfaces with a higher roughness. However, in this case, the contact angle values are more dependent on the chemistry of the samples than on the surface morphology.

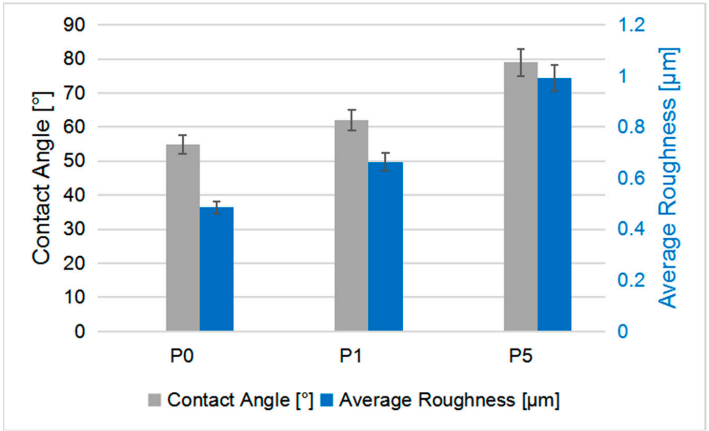

Figure 7. Contact angle and surface roughness values.

4. Discussion

Particles with ζ-potentials higher than +30 mV or lower than −30 mV are considered to have moderate stability, while high stability is generally ensured by ζ-potential values more negative than −50 mV or more positive than 50 mV [54]. These values can ensure a sufficient electrostatic repulsion to generate stability over a longer period of time.

Particles suspended in the fluid medium are influenced by the interaction of three different forces: the van der Waals force of attraction, the electrostatic repulsion force and the steric (polymeric) force (not always present). To have a stable suspension, repulsive electrostatic and/or steric forces must be dominant against the van der Waals force that tries to agglomerate the particles. Another way to improve the suspendibility of particles is the interaction with polyelectrolytes (e.g., chitosan). If the polyelectrolyte has an opposite charge compared to the solid surface particle, the polyelectrolyte and the particle can bind to each other. The rest of the polymer chain acts as a micelle around the particle, increasing the suspending capacity, while its chain holds the other polymer chains apart through electrosteric forces (steric repulsion) [55].

Three types of samples were prepared and characterized: etched 73Ti-20Zr-5Ta-2Ag (P0), etched 73Ti-20Zr-5Ta-2Ag covered only with chitosan (P1) and etched 73Ti-20Zr-5Ta-2Ag covered with the Chi:(BG:ZnO) mixture which showed the greatest stability (P5).

Sample P0 was covered with complex oxides (Figure 4a,a') resulting from the etching process formed mainly from Ti and Zr, as evidenced by the EDX (Figure 5a) and FT-IR (Figure 6). The presence of Ag particles scattered on the surface indicates that the alloy is not homogeneous at a micro-level. The grooves and pores present on the surfaces of the alloy samples are the result of the competition between the processes of oxide forming and oxide dissolution. The shapes of these structures are characteristic of TiZr alloys [56].

At low magnifications (Figure 4b), sample P1 was found to be covered completely with a thin chitosan film, which became transparent for the SEM electron beam at higher magnifications. The structures shown at higher magnifications (Figure 4b') are those of the etched Ti-Zr-Ta-Ag sample and are similar to those found on sample P0. The evidence for the chitosan film comes from the EDX (Figure 5b), where a carbon peak was recorded and FT-IR (Figure 6) analysis where the recorded spectrum of P1 was virtually identical to the one recorded for pure chitosan.

Sample P5 (Figure 4c,c') was found to be homogeneous, with a good dispersion of ceramic particles present in the chitosan film. Only the smaller particles seem to have been deposited on the sample, the larger particles probably being too heavy to be transported by the electrical field during the electrospinning process. Some agglomeration was expected to take place during the slow drying process, resulting in observed particles being larger than those recorded during the DLS measurements. The composition detected by the EDX (Figure 5c) shows the presence of all the ceramic components.

A slight peak shift in the region pf 1645 cm^{-1} attributed to N-H bending hints that the chitosan forms complexes with the introduced ceramic elements [57].

The variation in the contact angles and roughness values could be discussed, taking into account the conclusion of the selected acid pretreatment of the alloy substrate based on recently acquired knowledge [58]. As expected, the contact angle values of the coated samples are in the hydrophilic domain but higher compared to the uncoated alloy values. Such behavior is promising for better adherence to cells in a future bioapplication [59].

5. Conclusions

Mixtures containing different amounts of chitosan, bioglass and ZnO were fabricated and analyzed. DLS and ζ-potentials measurements determined that the most stable mixture had the component ratio 2Chi:1(1BG:5ZnO) and had the smallest suspended particle size and the most positive potential. This mixture was deposited on previously etched 73Ti-20Zr-5Ta-2Ag alloy samples and further analyzed. SEM analysis revealed that the coated sample had good homogeneity. EDX analysis corroborated with FT-IR spectroscopy revealed that all the ceramic components were present on the surface of the samples and that the chitosan

formed complexes with metals from the solid components of the mixture. The contact angle values are higher for the coated samples but remain in the hydrophilic domain as a usual characteristic for bioactive and biocompatible coatings. The rougher surfaces obtained after coating are a promoter for better cell adherence, a condition of osseointegration process and good implant behavior.

Author Contributions: Conceptualization, D.I., I.D. and M.E.; methodology, D.I., M.E., M.P. and A.B.S.; writing—original draft preparation, M.P. and A.B.S.; organized the whole research paper, D.I., M.P. and I.D.; designed the working approach, D.I.; wrote the main aspects, A.B.S.; writing—review and editing, G.V.M. and M.E.; SEM and EDX characterization, G.V.M.; supervision, I.D. and M.E. All authors have read and agreed to the published version of the manuscript.

Funding: This research was funded by the Executive Agency for Higher Education, Research, Development and Innovation Funding, Grant No. PN-III-P2-2.1-PED-2021-2884 (605PED/2022). This research was funded by ECSEL JU under the following grant agreements: No. 826422 (PIn3S), No. 876124 (BEYOND5) and No. 875999 (IT2). The JU receives support from the European Union's Horizon 2020 research and innovation program and Italy, Switzerland, Germany, Belgium, Sweden, Austria, Romania, Slovakia, France, Poland, Spain, Ireland, Israel, Portugal, Greece, Netherlands, Hungary, United Kingdom. This work is financially supported by the Romanian Ministry of Research, Innovation and Digitalization, under the following ECSEL—H2020 Projects: PIn3S—Contract no. 10/1.1.3H/03.04.2020, POC-SMIS code 135127, BEYOND5—Contract no. 12/1.1.3/31.07.2020, POC-SMIS code 136877 and IT2—Contract. no. 11/1.1.3H/06.07.2020, POC-SMIS code 136697.

Institutional Review Board Statement: Not applicable.

Informed Consent Statement: Not applicable.

Data Availability Statement: Not applicable.

Conflicts of Interest: The authors declare no conflict of interest.

References

1. Boyer, R.R. Titanium for aerospace: Rationale and applications. *Adv. Perform. Mater.* **1995**, *2*, 349–368. [CrossRef]
2. Andijani, I.N.; Ahmad, S.; Malik, A.U. Corrosion behavior of titanium metal in the presence of inhibited sulfuric acid at 50 °C. *Desalination* **2000**, *129*, 45–51. [CrossRef]
3. Schutz, R.W. Utilizing titanium to successfully handle chloride process environments. *CIM Bull.* **2002**, *95*, 84–88.
4. Wang, C.P.; Wang, H.; Ruan, G.; Wang, S.; Xiao, Y.; Jiang, L. IOP Applications and prospects of titanium and its alloys in seawater desalination industry. *Conf. Ser. Mater. Sci. Eng.* **2019**, *688*, 033036–033043. [CrossRef]
5. Prando, D.; Brenna, A.; Diamanti, M.V.; Beretta, S.; Bolzoni, F.; Ormellese, M.; Pedeferri, M.P. Corrosion of titanium: Part 1: Aggressive environments and main forms of degradation. *J. Appl. Biomater. Funct. Mater.* **2017**, *15*, e291–e302. [CrossRef] [PubMed]
6. Shen, Y.; Fang, K.; Xiang, Y.; Xu, K.; Yu, L.; Chen, J.; Ma, P.; Cai, K.; Shen, X.; Liu, J. Improvement in osteogenesis, vascularization, and corrosion resistance of titanium with silicon-nitride doped micro-arc oxidation coatings. *J. Front. Bioeng. Biotechnol.* **2022**, *10*, 1023032–1023046. [CrossRef]
7. Rodrigues, D.C.; Valderrama, P.; Wilson, T.G.; Palmer, K.; Thomas, A.; Sridhar, S.; Adapalli, A.; Burbano, M.; Wadhwani, C. Titanium corrosion mechanisms in the oral environment: A retrieval study. *Materials* **2013**, *6*, 5258–5274. [CrossRef]
8. *ASTM Designation F136-82*; Standard Specification for Wrought Titanium 6Al 4V ELI Alloy for Surgical Implants. ASTM: Philadelphia, PA, USA, 1994; pp. 19–20.
9. *ASTM Designation F1295-92*; Standard Specification for Wrought Titanium 6Al 7Nb Alloy for Surgical Implants. ASTM: Philadelphia, PA, USA, 1994; pp. 687–689.
10. Popa, M.V.; Demetrescu, I.; Vasilescu, E.; Drob, P.; Ionita, D.; Vasilescu, C. Stability of some dental implant materials in oral biofluids. *Rev. Roum. De Chim.* **2005**, *50*, 399–406.
11. Akimoto, T.; Ueno, T.; Tsutsumi, Y.; Doi, H.; Hanawa, T.; Wakabayashi, N. Evaluation of corrosion resistance of implant-use Ti-Zr binary alloys with a range of compositions. *J. Biomed. Mater. Res. B* **2018**, *106 Pt B*, 73–79. [CrossRef]
12. Ionita, D.; Pirvu, C.; Stoian, A.B.; Demetrescu, I. The Trends of TiZr Alloy Research as a Viable Alternative for Ti and Ti16 Zr Roxolid Dental Implants. *Coatings* **2020**, *10*, 422. [CrossRef]
13. Cantor, B.; Chang, I.T.H.; Knight, P.; Vincent, A.J.B. Microstructural development in equiatomic multicomponent alloys. *Mater. Sci. Eng. A* **2004**, *375–377*, 213–218. [CrossRef]
14. Yeh, J.W.; Chen, S.K.; Lin, S.J.; Gan, J.Y.; Chin, T.S.; Shun, T.T.; Tsau, C.H.; Chang, S.Y. Nanostructured high-entropy alloys with multiple principal elements: Novel alloy design concepts and outcomes. *Adv. Eng. Mater.* **2004**, *6*, 299–303. [CrossRef]

15. Geantă, V.; Voiculescu, I.; Istrate, B.; Vrânceanu, D.; Ciocoiu, R.; Cotruț, C. The influence of chromium content on the structural and mechanical properties of AlCrxFeCoNi high entropy alloys. *Int. J. Eng. Res. Afr.* **2018**, *37*, 23–28. [CrossRef]
16. Vasilescu, E.V.; Calderon, M.J.M.; Vasilescu, C.; Drob, S.I.; Stanciu, D.E.; Ivanescu, S.; Ionita, M.D.; Prodana, M. Ti-Zr-Ta-Ag Bio-alloy for Orthopedic Implants OSIM. Bucuresti. Patent 132031, 30 April 2019.
17. Vasilescu, C.; Drob, S.; Osiceanu, P.; Moreno, J.M.C.; Prodana, M.; Ionita, D.; Demetrescu, I. Microstructure, surface characterization, and electrochemical behavior of new Ti-Zr-Ta-Ag alloy in simulated human electrolyte. *Metall. Mater. Trans. A* **2017**, *48*, 513–523. [CrossRef]
18. Manole, C.C.; Pirvu, C.; Stoian, A.B.; Calderon Moreno, J.M.; Stanciu, D.; Demetrescu, I. The electrochemical stability in NaCl solution of nanotubes and nanochannels elaborated on a new Ti-20Zr-5Ta-2Ag alloy. *J. Nanomater.* **2015**, *8*, 41. [CrossRef]
19. Vasilescu, C.; Osiceanu, P.; Moreno, J.M.C.; Drob, S.I.; Preda, S.; Popa, M.; Dan, I.; Marcu, M.; Prodana, M.; Popovici, I.A.; et al. Microstructure, surface characterization and long-term stability of new quaternary Ti-Zr-Ta-Ag alloy for implant use. *Mater. Sci. Eng. C* **2017**, *71*, 322–334. [CrossRef]
20. Xie, J.; Luan, B.L. Formation of hydroxyapatite coating using novel chemo-biomimetic method. *J. Mater. Sci. Mater. Med.* **2008**, *19*, 3211–3220. [CrossRef]
21. Ionita, D.; Vardaki, M.; Stan, M.S.; Dinischiotu, A.; Demetrescu, I. Enhance stability and in vitro cell response to a bioinspired coating on zr alloy with increasing chitosan content. *J. Bionic. Eng.* **2017**, *14*, 459–467. [CrossRef]
22. Prodana, M.; Stoian, A.B.; Burnei, C.; Ionita, D. Innovative Coatings of Metallic Alloys Used as Bioactive Surfaces in Implantology: A Review. *Coatings* **2021**, *11*, 649. [CrossRef]
23. Heimann, R.B. The challenge and promise of low-temperature bioceramic coatings: An editorial. *Surf. Coat. Technol.* **2016**, *301*, 1–5. [CrossRef]
24. Monsalve, M.; Lopez, E.; Ageorges, H.; Vargas, F. Bioactivity and mechanical properties of bioactive glass coatings fabricated by flame spraying. *Surf. Coat. Technol.* **2015**, *268*, 142–146. [CrossRef]
25. Dou, Y.; Cai, S.; Ye, X.; Xu, G.; Huang, K.; Wang, X.; Ren, M. 45S5 bioactive glass–ceramic coated AZ31 magnesium alloy with improved corrosion resistance. *Surf. Coat. Technol.* **2013**, *228*, 154–161. [CrossRef]
26. Seuss, S.; Heinloth, M.; Boccaccini, A.R. Development of bioactive composite coatings based on combination of PEEK, bioactive glass and Ag nanoparticles with antibacterial properties. *Surf. Coat. Technol.* **2016**, *301*, 100–105. [CrossRef]
27. Córdoba, L.C.; Marques, A.; Taryba, M.; Coradin, T.; Montemor, F. Hybrid coatings with collagen and chitosan for improved bioactivity of Mg alloys. *Surf. Coat. Technol.* **2018**, *341*, 103–115. [CrossRef]
28. Cordero-Arias, L.; Boccaccini, A. Electrophoretic deposition of chondroitin sulfate chitosan/bioactive glass composite coatings with multilayer design. *Surf. Coat. Technol.* **2017**, *315*, 417–425. [CrossRef]
29. Radda'a, N.S.; Goldmann, W.H.; Detsch, R.; Roether, J.A.; Cordero-Arias, L.; Virtanen, S.; Moskalewicz, T.; Boccaccini, A.R. Electrophoretic deposition of tetracycline hydrochloride loaded halloysite nanotubes chitosan/bioactive glass composite coatings for orthopedic implants. *Surf. Coat. Technol.* **2017**, *327*, 146–157. [CrossRef]
30. Mocanu, A.-C.; Miculescu, F.; Dascalu, C.-A.; Voicu, S.I.; Pandele, M.-A.; Ciocoiu, R.-C.; Batalu, D.; Dondea, S.; Mitran, V.; Ciocan, L.-T. Influence of Ceramic Particles Size and Ratio on Surface—Volume Features of the Naturally Derived HA-Reinforced Filaments for Biomedical Applications. *J. Funct. Biomater.* **2022**, *13*, 199. [CrossRef]
31. Weiner, S.; Wagner, H.D. The material bone: Structure-mechanical function relations. *Annu. Rev. Mater. Sci.* **1998**, *28*, 271–298. [CrossRef]
32. Meyer, N.; Rivera, L.R.; Ellis, T.; Qi, J.H.; Ryan, M.P.; Boccaccini, A.R. Bioactive and Antibacterial Coatings Based on Zein/Bioactive Glass Composites by Electrophoretic Deposition. *Coatings* **2018**, *8*, 27. [CrossRef]
33. Nartita, R.; Ionita, D.; Demetrescu, I. Sustainable Coatings on Metallic Alloys as a Nowadays Challenge. *Sustainability* **2021**, *13*, 10217. [CrossRef]
34. Hench, L.L.; Splinter, R.J.; Allen, W.; Greenlee, T. Bonding mechanisms at the interface of ceramic prosthetic materials. *J. Biomed. Mater. Res.* **1971**, *5*, 117–141. [CrossRef]
35. Maximov, M.; Maximov, O.-C.; Craciun, L.; Ficai, D.; Ficai, A.; Andronescu, E. Bioactive Glass—An Extensive Study of the Preparation and Coating Methods. *Coatings* **2021**, *11*, 1386. [CrossRef]
36. Durand, L.A.H.; Vargas, G.E.; Romero, N.M.; Vera-Mesones, R.; Porto-López, J.M.; Boccaccini, A.R.; Zago, M.P.; Baldi, A.; Gorustovich, A. Angiogenic effects of ionic dissolution products released from a boron-doped 45S5 bioactive glass. *J. Mater. Chem. B* **2015**, *3*, 1142–1148. [CrossRef] [PubMed]
37. Rabea, E.I.; Badawy, M.E.-T.; Stevens, C.V.; Smagghe, G.; Steurbaut, W. Chitosan as antimicrobial agent: Applications and mode of action. *Biomacromolecules* **2003**, *4*, 1457–1465. [CrossRef] [PubMed]
38. Boccacini, A.R.; Dickerson, J. Electrophoretic deposition Fundamentals and Applications. *Phys. Chem. B* **2013**, *117*, 1501. [CrossRef]
39. Pishbin, F.; Simchi, A.; Ryan, M.; Boccaccini, A. Electrophoretic deposition of chitosan/45S5 Bioglass® composite coatings for orthopaedic applications. *Surf. Coat. Technol.* **2011**, *205*, 5260–5268. [CrossRef]
40. Pishbin, F.; Mouriño, V.; Gilchrist, J.; McComb, D.; Kreppel, S.; Salih, V.; Ryan, M.P.; Boccaccini, A.R. Single-step electrochemical deposition of antimicrobial orthopaedic coatings based on a bioactive glass/chitosan/nano-silver composite system. *Acta Biomater.* **2013**, *9*, 7469–7479. [CrossRef] [PubMed]

41. Zhitomirsky, D.; Roether, J.; Boccaccini, A.; Zhitomirsky, I. Electrophoretic deposition of bioactive glass/polymer composite coatings with and without HA nanoparticle inclusions for biomedical applications. *J. Mater. Process. Technol.* **2009**, *209*, 1853–1860. [CrossRef]
42. Badiceanu, M.; Anghel, S.; Mihailescu, N.; Visan, A.I.; Mihailescu, C.N.; Mihailescu, I.N. Coatings Functionalization via Laser versus Other Deposition Techniques for Medical Applications: A Comparative Review. *Coatings* **2022**, *12*, 71. [CrossRef]
43. Khademi, M.; Wang, W.; Reitinger, W.; Barz, D.P.J. Zeta Potential of Poly (methyl methacrylate) (PMMA) in Contact with Aqueous Electrolyte-Surfactant Solutions. *Langmuir* **2017**, *33*, 10473–10482. [CrossRef]
44. Salami, R.; Arami, M.; Mohammad, N.; Bahrami, H.; Khorramfar, S. Novel biocompatible composite (Chitosan-zinc oxide nanoparticle): Preparation, charaterization and dye adsorption properties. *Colloids Surf. B* **2010**, *80*, 86–93.
45. Lin, M.H.; Wang, Y.H.; Kuo, C.H.; Ou, S.F.; Huang, P.Z.; Song, T.Y.; Chen, Y.C.; Chen, S.T.; Wu, C.H.; Hsueh, Y.H.; et al. Hybrid ZnO/chitosan antimicrobial coatings with enhanced mechanical and bioactive properties for titanium implants. *Carbohydr. Polym.* **2021**, *257*, 117639. [CrossRef] [PubMed]
46. Maci, F.; Moskalewicz, T.; Kowalski, K.; Łukaszczyk, A.; Hadzhieva, Z.; Boccaccini, A.R. The Effect of Electrophoretic Deposition Parameters on the Microstructure and Adhesion of Zein Coatings to Titanium Substrates. *Materials* **2021**, *14*, 312–336.
47. Cunha, A.G.; Fernandes, S.C.M.; Friere, C.S.R.; Silvestre, A.J.C.; Neto, C.P.; Gandini, A. What is the real value of chitosan's surface energy? *Biomacromolecules* **2008**, *9*, 610–614. [CrossRef]
48. Kim, K.M.; Choi, M.H.; Lee, J.K.; Jeong, J.; Kim, Y.R.; Kim, M.K.; Paek, S.M.; Oh, J.M. Physicochemical properties of surface charge-modified ZnO nanoparticles with different particle sizes. *Int. J. Nanomed.* **2014**, *9* (Suppl. S2), 41–56.
49. Aibani, N.; Rai, R.; Patel, P.; Cuddihy, G.; Wasan, E.K. Chitosan Nanoparticles at the Biological Interface: Implications for Drug Delivery. *Pharmaceutics* **2021**, *3*, 1686. [CrossRef]
50. Kampstra, P. Beanplot: A Boxplot Alternative for Visual Comparison of Distributions. *J. Stat. Soft.* **2008**, *28*, 1–9. [CrossRef]
51. IR Spectrum Table & Chart. Available online: https://www.sigmaaldrich.com/RO/en/technical-documents/technical-article/analytical-chemistry/photometry-and-reflectometry/ir-spectrum-table (accessed on 29 January 2023).
52. Tabia, Z.; El Mabrouk, K.; Bricha, M.; Nouneh, K. Mesoporous bioactive glass nanoparticles doped with magnesium: Drug delivery and acellular in vitro bioactivity. *RSC Adv.* **2019**, *9*, 12232–12246. [CrossRef]
53. Gonçalves, R.V.; Wojcieszak, R.; Uberman, P.M.; Teixeira, S.R.; Rossi, L.M. Insights into the active surface species formed on Ta2O5 nanotubes in the catalytic oxidation of CO. *Phys. Chem. Chem. Phys.* **2014**, *16*, 5755–5762. [CrossRef]
54. Joseph, E.; Singhvi, G. *Chapter 4-Multifunctional Nanocrystals for Cancer Therapy: A Potential Nanocarrier, Nanomaterials for Drug Delivery and Therapy*; William Andrew Publishing: Norwich, NY, USA, 2019; pp. 91–116. ISBN 9780128165058.
55. Liang, Y.; Hilal, N.; Langston, P.; Starov, V. Interaction forces between colloidal particles in liquid: Theory and experiment. *Adv. Colloid Interface Sci.* **2007**, *134–135*, 151–166. [CrossRef]
56. Wang, B.; Ruan, W.; Liu, J.; Zhang, T.; Yang, H.; Ruan, J. Microstructure, mechanical properties, and preliminary biocompatibility evaluation of binary Ti–Zr alloys for dental application. *J. Biomater. Appl.* **2019**, *33*, 766–775. [CrossRef]
57. Chen, Y.; Cai, J.; Liu, D.; Liu, S.; Lei, D.; Zheng, L.; Wei, Q.; Gao, M. Zinc-based metal organic framework with antibacterial and anti-inflammatory properties for promoting wound healing. *Regen. Biomater.* **2022**, *9*, rbac019. [CrossRef] [PubMed]
58. Nartita, R.; Ionita, D.; Demetrescu, I.; Enachescu, M. selecting a surface preparation treatment on a medium entropy Ti-Zr-Ta-Ag alloy. *Annal. Acad. Rom. Sci.-Ser. Phys. Chem.* **2021**, *6*, 23–30. [CrossRef]
59. Ferrari, M.; Cirisano, F.; Morán, M.C. Mammalian Cell Behavior on Hydrophobic Substrates: Influence of Surface Properties. *Colloids Interfaces* **2019**, *3*, 48. [CrossRef]